Communication • DOI: 10.2478/v10134-010-0019-6 • Translational Neuroscience • 1(2) •2010 •131–138

Translational Neuroscience

VERSITA

CINGULUM BUNDLE WHITE MATTER IN MAG-KNOCKOUT MICE

Devorah Segal[1]*,
David Carpenter[2],
Malin Höistad[1],
Vahram Haroutunian[3],
Cheuk Y. Tang[2,3],
Patrick R. Hof[1]

Departments of [1]Neuroscience, [2]Radiology, and [3]Psychiatry, Mount Sinai School of Medicine, New York, NY 10029, USA

Abstract

Myelin associated glycoprotein (MAG) is an oligodendrocyte-derived gene whose expression is decreased in schizophrenia. Several measures of white matter integrity appear abnormal in schizophrenia, specifically in the anterior cingulate gyrus. We studied mice lacking MAG as a potential model of dysmyelination. Using the stereological "Space Balls" method, we estimated myelinated fiber length density in the cingulum bundle in adult knockout and control mice. We performed diffusion anisotropy imaging in these animals, measuring fractional anisotropy (FA) in a region of the cingulum bundle. We found no differences in cingulum myelinated fiber length density between the two groups, although we did note an age-related decrease regardless of genotype. No differences were noted in FA either, but an age-related decrease was seen as well. These findings imply that MAG dysfunction alone is not sufficient to cause the white matter alterations seen in schizophrenia.

Keywords

MAG • Cingulum bundle • Stereology • DTI • Schizophrenia • Mouse model

Received 7 June 2010
accepted 17 June 2010

1. Introduction

Evidence from gene expression studies in schizophrenia have demonstrated decreased expression of several oligodendrocyte-derived genes, including myelin associated glycoprotein (MAG) [1,2]. A gene linkage study also found that polymorphisms in the MAG gene were associated with schizophrenia [3]. Postmortem investigations have shown fewer oligodendrocytes in the prefrontal cortex in schizophrenia [4,5], and an electron microscopy study has demonstrated abnormal oligodendrocytes and myelin sheaths, as well [6]. Several structural magnetic resonance imaging (MRI) studies show a decrease in the area of the corpus callosum [7], and a postmortem study suggested decreased callosal fiber length in women with schizophrenia [8]. Decreased anisotropy has been reported in several white matter regions in schizophrenia [9-16], further implying dysfunction of white matter tracts. The combined evidence for a white matter abnormality has led some to suggest that schizophrenia may be a disease of altered wiring [17,18], and that white matter plays a crucial role in the symptoms of schizophrenia.

The anterior cingulate gyrus has become a region of interest in schizophrenia research. The human anterior cingulate cortex (ACC) has connections with the amygdala, orbitofrontal cortex, and entorhinal cortex and plays a role in conditioned emotional learning, information processing, motivation, and behavior [19]. Several myelin-related genes, including the oligodendrocyte-derived MAG, have decreased expression levels in the ACC [20-22], and fewer glial cells have been noted in the ACC in schizophrenia [23]. The cingulum bundle is the major white matter tract in the cingulate gyrus and carries fibers connecting the parahippocampal gyrus and the orbitofrontal cortex, as well as fibers radiating to the striatum, thalamus, and internal capsule [24,25]. DTI studies have demonstrated decreased anisotropy in the cingulum bundle in schizophrenia [26-30]. Anisotropy changes in men with schizophrenia have been noted in a number of brain areas, including the anterior cingulate gyrus, and were specifically linked to increased impulsivity, a symptom of the disease [11]. Adolescents with early onset schizophrenia, a particular form of the disorder, show decreased anisotropy in the left anterior cingulate gyrus as well [31,32]. One recent study found no diffusion anisotropy differences in the cingulum bundle between patients and controls, but reported a relative increase in diffusion anisotropy in the cingulum bundle of patients with auditory hallucinations compared to those without [16].

In the present study, we examined two measures of white matter integrity in a genetically altered mouse model in which the myelin-related gene MAG has been knocked out. Selected because of its decreased expression levels [1,2,22] and status as a susceptibility gene in schizophrenia [3], MAG interacts with neuronal membranes and helps maintain the periaxonal space of

* *E-mail: devorah.segal@mssm.edu*

myelin sheaths [33]. Previously published studies have described various developmental abnormalities in the MAG-knockout model but have not demonstrated a clearly dysfunctional phenotype [33-38]. Subtle behavioral abnormalities in mice missing the MAG gene are decreased proficiency in maintaining balance on a rotating cylinder, hyperactivity, and impaired hindlimb reflex extension [38]. However, the mutant mice showed no differences in spatial learning and memory or in swimming speed, as demonstrated by a Morris water maze test [37]. MAG has been shown to inhibit neurite outgrowth and impair axonal regeneration and may be involved in maintaining healthy axons [39]. These mice may also exhibit some alterations of pyramidal cell dendritic branching patterns [40]. MAG-knockout mice may therefore have disruptions in normal myelinated tract development that are reflected in altered anisotropy or fiber length density. The MAG-knockout mouse may thus serve as a model for examining the effects of impaired expression of a myelin-related protein linked to schizophrenia on a brain region affected in the disease. We therefore examined the cingulum bundle in these mice, using both DTI to examine white matter coherence and histological techniques to measure myelinated fiber length density.

2. Experimental Procedures

2.1 Animals

Sixteen C57BL/6j mice, 9 MAG-knockout mice and 7 littermate controls were used. Mice were aged 8-17 months (Table 1), and we included one heterozygote in the control group, as there is no known heterozygous phenotype for this gene. Animals were deeply anesthetized with 30% (400 mg/kg) chloral hydrate i.p. The chest was opened to expose the heart, and they were perfused transcardially with cold 1% paraformaldehyde in phosphate-buffered saline (PBS; pH 7.4), followed by fixation with cold 4% paraformaldehyde for 12 minutes. The brain was removed from the skull and postfixed 6 hours to overnight in the same fixative and then transferred to buffer. All procedures were performed according to the NIH guidelines on experimental animal welfare and with the approval of the Institutional Animal Care and Use Committee of the Mount Sinai School of Medicine.

2.2 Diffusion tensor imaging

After postfixation, the mouse brains were washed in PBS and carefully dried to remove remaining PBS or fixative. They were then placed in a 10-mm polyethylene tube filled with fomblin (perfluoropolyether, Ausimont, Morristown, NJ), used to seal the specimen, preventing dehydration, and also to prevent susceptibility effects. All magnetic resonance microscopy scans were performed on a 9.4 T Bruker small vertical bore magnet (Bruker Biospin, Karlsruhe, Germany). An actively shielded gradient coil set was used with gradient strengths of up to 100 G/cm. A RF birdcage coil with a 10-mm inner diameter was used to scan the specimens. DTI was acquired using a Pulsed Gradient Spin Echo sequence with the following parameters: FOV = 16 mm, matrix size 128x128, 32 slices 0.5 mm-thick, no skip; TR = 16 s, TE = 20 ms. Six gradient directions were used with b-values of 1200 s/mm^2 and 14 averages. Fractional anisotropy (FA) maps were computed using in-house developed software using Matlab 7.1 (The Mathworks, Natick, MA, USA).

The processed FA maps were then viewed using DTIStudio software (version 2.4, Johns Hopkins University, Baltimore, MD, USA). All analyses were performed blind to genotype. For each mouse, a single slice was chosen to represent best the cingulum bundle. On the selected slices, the corpus callosum crossed the midline and no prominent hippocampus was seen, thus paralleling the region studied with stereology. The cingulum bundle was identified in the FA images by comparison to histological slices and an online mouse DTI atlas (http://www.birncommunity.org/data-catalog/mouse-diffusion-tensor-imaging-dti-atlas-of-developing-mouse-brains) [41]. The left and right cingulum bundles were traced on each chosen slice using the ROI function of DTIStudio (Figure 1), which provides the area of the traced region, along with the minimum, mean, and maximum FA, and standard deviation.

2.3 Stereology

Following DTI, the brains were hemisected, with one hemisphere used for the present stereological study. The hemisphere was embedded in agarose and cut in serial 50 μm-thick coronal sections using a Leica VT1000 S vibrating blade microtome (Leica, Wetzlar, Germany). One knockout mouse brain was

Table 1. Mice used for diffusion tensor imaging and stereological analyses.

Mouse	Age (months)	Sex	Cut hemisphere
KO1	11	F	L
KO2	10	F	R
KO3	8	F	R
KO4	11	M	N/A
KO5	14	M	R
KO6	15	M	R
KO7	15	M	L
KO8	15	F	L
KO9	17	F	L
HZ1	11	F	R
WT1	8	M	L
WT2	11	F	R
WT3	14	F	R
WT4	14	F	L
WT5	15	F	L
WT6	8	F	L

WT - wildtype; KO - knockout; HZ - heterozygous; F - female; M - male; L - left; R - right

not suitable for stereological investigations because of damage that occurred after DTI, so 8 MAG-knockout mice were included in the stereological analysis. Sections of the cingulum bundle were collected beginning at the plane where the corpus callosum crossed the midline and ending where the hippocampus became noticeable [42]. Every sixth section was then selected, beginning at a random section within the first six sections, and mounted on 2% gelatin-coated slides. Mounted sections were then stained using Black Gold (Histo-Chem Inc., Jefferson, Arkansas, USA) to stain myelin, as previously described [43], then dehydrated and coverslipped using DPX (Serva, Heidelberg, Germany). The mouse cingulum bundle was clearly identifiable as a roughly triangular region of dense fibers dorsal to the corpus callosum [42] (Figure 2). The border between the corpus callosum and the cingulum bundle was demarcated by the fiber direction: mediolateral in the corpus callosum and curving dorsally or anteroposteriorly in the cingulum bundle.

To reduce bias, all analyses were performed blind to genotype. For spatial analyses, Black Gold-stained sections (every 6th cut section) were first viewed at low magnification (10x) to outline the cingulum bundle using a Zeiss Axioplan 2 microscope and StereoInvestigator software (MBF Bioscience, Williston, VT). Myelinated fiber length density was then examined using the software's Space Balls probe [44-47]. The dimensions of the random sampling grid were set to place approximately 200 hemispheres throughout the outlined region (mean number of sampling sites = 229). Hemispheres with a radius of 6 μm were systematically and randomly placed by the stereology software, with a 0.5 μm guard zone at the top of the tissue to avoid counting in the compromised cut surface. The remainder of the tissue served as a bottom guard zone; mean section thickness was 17.9 μm. Myelinated fiber length density, defined as fiber length per unit of white matter volume, was calculated from the number of intersections between fibers and hemispheres (mean number of counted intersections = 4,085), using a 100x Zeiss PlanApo objective, 1.4 n.a. When using stereologic techniques on processed tissue, tissue volume change is always of concern. In this study, tissue sections were mounted soon after cutting and before staining, which minimizes shrinkage in the x–y directions [48]. Shrinkage in the z-direction can be substantial; the stereology software corrects for this by measuring the true section thickness at regular intervals and using this corrected thickness factor in calculating fiber length densities.

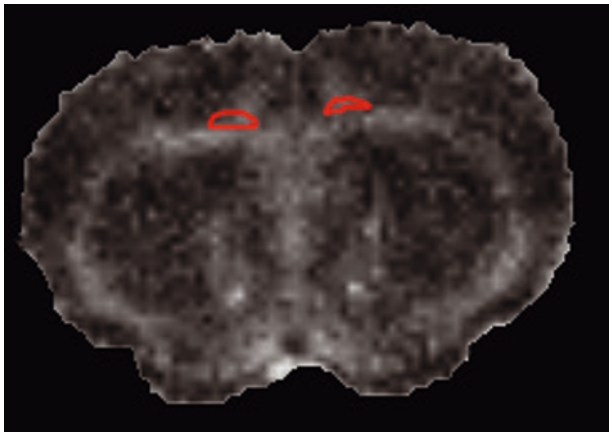

Figure 1. Example of the cingulum bundle traced in DTIstudio on an FA image.

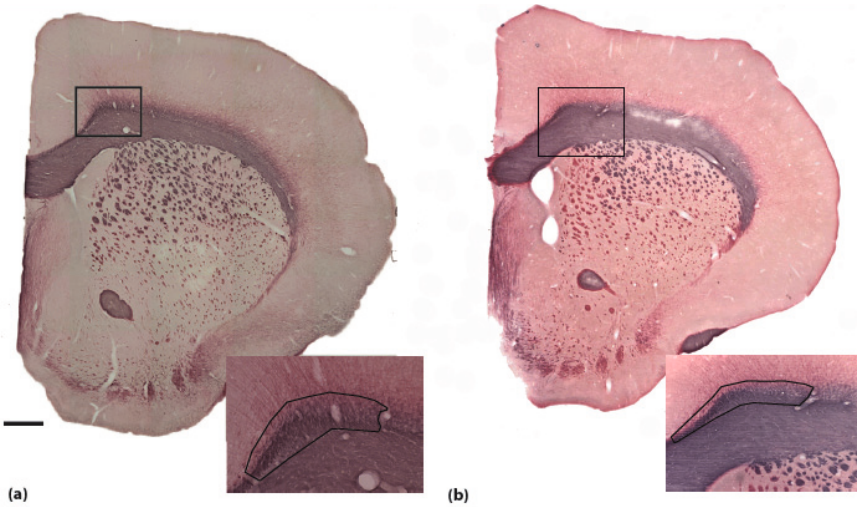

Figure 2. Low magnification (10x) images of a section from a (a) wildtype and (b) MAG-knockout mouse brain. Boxes show area magnified in inset. Inset shows outlined cingulum bundle. Scale bar = 50 mm for both.

2.4 Statistics

Group differences in age were assessed using the Student's *t* test. To include possible effects of age and hemisphere, mean fiber length densities in the cingulum bundle were compared for knockout and wildtype mice using a generalized linear model analysis of covariance (ANCOVA), with fiber length density as the dependent variable, genotype and hemisphere as categorical predictors, and age as a continuous covariate. FA values in the cingulum bundle were compared for knockout and wildtype mice using a generalized linear model repeated measures analysis of covariance (ANCOVA), with left and right minimum, maximum, and mean FA measures as the dependent variables; genotype and sex as categorical predictors; and age as a continuous covariate. Post-hoc tests (age, thickness) were performed with linear regression analysis, and fiber length density and FA were correlated with age or section thickness using Pearson's correlations. Slopes

were compared using the formula $t = (b_1\text{-}b_2)/(s_{b1\text{-}b2})^{1/2}$. All statistical analyses were performed using Statistica 6.1 (StatSoft Inc, Tulsa, OK), and statistical significance for all comparisons was set at $\alpha = 0.05$.

3. Results

3.1 Diffusion tensor imaging

Comparison of minimum, maximum, and mean FA in the cingulum bundle of MAG-knockout and wildtype control mice found no statistical significance between groups (Table 2). Mean FA in the right and left hemispheres did not differ between or within groups (ANOVA, p = 0.83). The area traced is likely not representative of the whole cingulum bundle volume in these mice, but it also did not differ between the two groups (ANOVA, p = 0.59), indicating that the sampled area was similar for wildtype and knockout mice. Although the mice in our study were all adults, their age range (8-17 months) led us to include age as a covariate in the ANCOVA. Surprisingly, age was the only significant predictor of FA in our analyses, regardless of genotype. Follow-up regression analysis revealed a decrease in FA in the cingulum with increasing age. This decrease was statistically significant in measures of right hemisphere maximum FA (r = -0.73, p = 0.002), right mean FA (r = -0.59, p = 0.017) left maximum FA (r = -0.55, p = 0.028), and left mean FA (r = -0.52, p = 0.038) (Figure 3).

3.2 Stereology

Comparison of myelinated fiber length density in the cingulum bundle in MAG-knockout mice and wildtype controls found no significant differences between groups (Table 3). Mean section thickness after staining and mounting did not differ between the two groups (mean section thickness was 19.7 μm for wildtype mice and 16.3 μm for knockout mice, p = 0.54), indicating that differential shrinkage did not occur. Additionally, there were no differences in mean number of sampling sites (wildtype mean = 238, knockout mean = 222; p = 0.67) or intersections counted (wildtype mean = 4,231, knockout mean = 3,957; p = 0.72). As with the DTI results, age was unexpectedly the only significant source of variance in the stereology results (p = 0.003). Follow-up regression analysis (Figure 4) showed a decrease in fiber length density in the cingulum bundle with increased age, an effect that was significant in both knockout mice (p = 0.028) and wildtype controls (p = 0.031). Comparison of the two

Table 2. Results of fractional anisotropy comparisons. Partial ANCOVA results are shown.

	Wildtype	Knockout
Mean right FA (x1000)	400.8	389.3
Mean left FA (x1000)	406.4	408.2
ANCOVA predictor of FA		**P value (F, df)**
Age		**0.01** (8.86, 1)
Genotype		0.45 (0.62, 1)
Sex		0.85 (0.04, 1)
Genotype x sex		0.91 (0.01, 1)
Hemisphere		0.99 (<0.001, 1)
Hemisphere x age		0.98 (<0.001, 1)
Hemisphere x genotype		0.99 (<0.001, 1)
Hemisphere x sex		0.74 (0.12, 1)
Hemisphere x genotype x sex		0.98 (<0.001, 1)

Significant p values are shown in bold type.

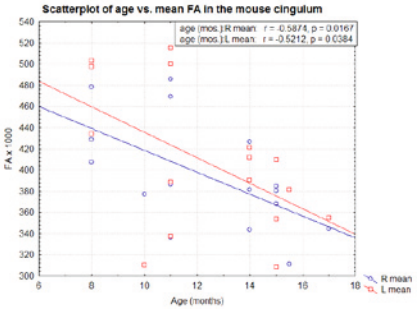

Figure 3. Scatterplots of age *vs.* mean FA in the left and right cingulum bundle in mice, with regression lines drawn and Pearson's r and p values indicated.

Table 3. Results of stereology and general linear model ANCOVA for fiber length density.

Mean density (μm/μm³)	**All mice**	**8 month-old mice excluded**
Wildtype	0.0749	0.0493
MAG knockout	0.0611	0.0550
ANCOVA predictor of fiber length density	**P value (F, df)**	**P value, section thickness included as covariate (F, df)**
Genotype	0.83 (0.05, 1)	0.43 (0.69, 1)
Hemisphere	**0.04** (5.58, 1)	0.21 (1.80, 1)
Genotype x hemisphere	0.23 (1.60, 1)	0.19 (1.97, 1)
Age	**0.003** (15.26, 1)	0.98 (0.004, 1)
Section mounted thickness		**<0.001** (142.56, 1)

Significant p values are shown in bold type.

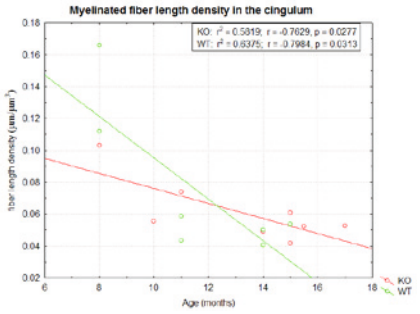

Figure 4. Scatterplots of age *vs.* fiber length density in the cingulum bundle, with regression lines drawn and Pearson's r and p values indicated. WT, wildtype controls; KO, knockout mice.

slopes did not reveal a significant difference between genotypes in the effect of age on fiber length density (b_1 = -0.013, b_2 = -0.005, t = -1.77, p = 0.105). Closer inspection revealed that the regression analysis was largely driven by three 8-month old mice, two wildtype and one knockout. Because of these apparent outliers, we repeated all analyses excluding the three younger mice. Again, there was no difference in fiber length density between the groups, and the age effect was no longer significant (data not shown). As it was noted that these younger mice had thicker sections, we repeated the ANCOVA with both age and section thickness as covariates. Here, section thickness was revealed to be a significant predictor of fiber length density, regardless of genotype, whereas age was not (Table 3). Further regression analysis showed an increase in fiber density with increased section thickness (p < 0.0001) as well as a correlation between section thickness and the age of the mice (p = 0.001) (Figure 5). Although mice of both sexes were included in our study, we could not include sex as factor in the ANCOVA model due to the presence of only one male wildtype control mouse. To rule out an effect of sex on fiber length density, an ANOVA was performed with hemisphere and sex as the categorical predictors, and not genotype. No effect was present for either sex (p = 0.60) or sex x hemisphere (p = 0.38).

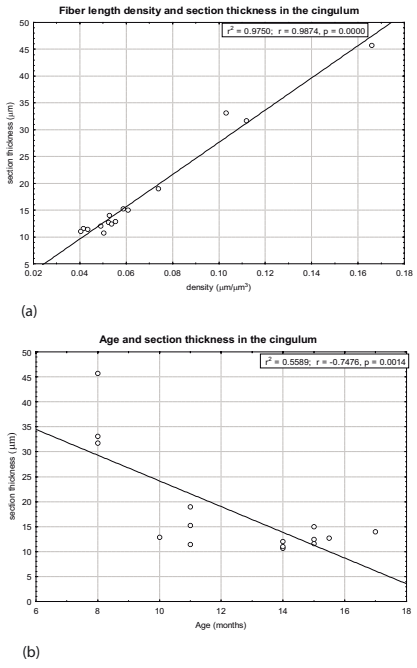

Figure 5. Scatterplots of (a) section thickness vs. fiber length density in the cingulum bundle, and (b) section thickness *vs.* mouse age. Regression lines are drawn and Pearson's r and p values are indicated.

Because both density and mean FA measures increased with age, we assessed whether there was a direct correlation between these measures. A regression analysis of myelinated fiber length density versus mean right and left FA measures showed a direct correlation between these measures (density: right mean FA, r = 0.581, p = 0.02; density: left mean FA, r = 0.682, p = 0.005, data not shown).

4. Discussion

Converging evidence suggests that myelin, and specifically oligodendrocytes, is in some way dysfunctional in schizophrenia [40,49,50]. In the present study, we used the MAG knockout mouse as a putative model for the dysmyelination that may occur in schizophrenia. Although the MAG-knockout mouse cannot be expected to show the distinctly human behavioral deficits of schizophrenia, it can serve as a vehicle for studying the morphological abnormalities resulting from a dysmyelinating genetic abnormality linked to the disease. A clear advantage of animal models is one we utilized in the present study: we were able to perform DTI and histology in the same brains. There is no indication of any sex-specific effect of the MAG gene [38], so our groups included both sexes. We also included one heterozygote mouse in our wildtype control group, because there is no indication of a heterozygote phenotype [33].

By using stereologic techniques to explore fiber length density and DTI to look at fractional anisotropy in the cingulum bundle, we hoped to gain a more complete understanding of the white matter pathology in the MAG-knockout mice, as well as finding a possible structural cellular correlate to DTI findings. Here, we found no differences in either fiber length density or FA between the knockout and wildtype mice. However, postmortem studies of myelinated fiber density in human subjects have largely found no differences between schizophrenia and controls. Fiber density studies in the corpus callosum [8] and the anterior commissure [51] showed a gender-specific decrease, present in women with schizophrenia, but not men, while a study of fiber density in the fornix found an increase in men with schizophrenia, but not women [52]. Another study looking at global and prefrontal myelinated fiber density in men with schizophrenia found no differences [53], as did studies of the uncinate fasciculus and corpus callosum in both men and women [54-56]. These studies are of particular importance given the presence of diffusion anisotropy abnormalities in many of the same regions, such as the corpus callosum [7]. The results reported here are therefore not entirely surprising given the lack of reports of large-scale myelin anomalies in schizophrenia. The myelin deficit of schizophrenia, like the deficit resulting from a lack of MAG, may be a fairly subtle one that does not manifest itself in a gross reduction in number of myelinated fibers. Similarly, we recently examined oligodendrocyte number, density, and spatial arrangement in the human cingulum bundle in schizophrenia [57], finding no differences in the disease. The decrease in oligodendrocyte-derived genes reported in schizophrenia is thus likely not a result of fewer oligodendrocytes, but a dysfunction of these cells. These MAG-deficient oligodendrocytes appear to be capable of myelinating the same number of axons as healthy cells, even though the sheaths themselves may be abnormal. In addition, the cingulum bundle may not be affected at all in schizophrenia, perhaps differing from other major white matter tracts, such as the corpus callosum, in this regard. Further ultrastructural studies should be conducted in brain white matter regions, such as the cingulum bundle, to investigate these possibilities.

An interesting and unexpected result in this study was the noted significant decrease in both myelinated fiber length density and FA in the cingulum bundle with increasing age. This decrease was noted regardless of genotype, hemisphere, or sex. The higher fiber density noted in younger mice is not likely attributable to the increased thickness of the mounted sections, resulting from less shrinkage during processing, as that would presumable result in decreased fiber density. The relationship between age and processed section thickness

must also be addressed, as the younger mice tended to have less tissue shrinkage in the z-direction in our findings. It is conceivable that younger mice have a truly increased myelinated fiber density in the cingulum, resulting in less free interaxonal space filled with water, and thus less shrinkage with the dehydration steps of our staining protocol, as well as increased measured fiber length density. Alternatively, younger mice may have healthier myelin which may stain better with Black Gold. This could lead to fuller penetration of the tissue, which would artificially inflate both the measured section thickness and the measured fiber density, which would skew the findings of stereologic studies. In addition, the space balls stereological technique, in particular, may be sensitive to section thickness, a possibility that should be explored further when using this technique.

Our parallel findings of increased FA in the cingulum in younger mice, however suggests a true age effect. Indeed, there is evidence for changes in myelinated fibers with aging, including myelin degeneration and loss of fibers [58]. One study of adult MAG-knockout mice found a dramatic increase in axonal pathology in aged mice, approximately 15-17 month old [34], although our findings in both knockout and wildtype mice do not support a gene-specific effect. Similarly, a recent study of FA in several white matter tracts in both young and old persons with schizophrenia found a decrease in FA with age in both the patients and healthy controls, a decline that was unchanged by the presence of disease [59]. In our study, lower FA and lower fiber density in older mice may be unrelated effects of aging, or the lower FA may be a functional reflection of decreased fiber density. We found that the two measures were highly correlated, suggesting that the decreased FA may be a direct reflection of the decreased fiber length density measured in these animals. At present, it is unknown whether decreases in anisotropy are due to fewer axons occupying the same space, to thinner myelin sheaths, or to some combination of these processes. A recent study of the brain of a Madagascan prosimian primate, the aye-aye (*Daubentonia madagascariensis)*, compared DTI and histological results and found strong correspondence in the measure of fiber spread obtained with these two very different methods [60]. We describe here a similar correspondence between anisotropy data and fiber length density in the mouse cingulum bundle.

By identifying the cingulum bundle on FA maps and tracing the region on those FA images, we introduced a limitation to the present study. Our method may bias the tracing to include only portions of the cingulum bundle that have increased FA compared to surrounding tissue. Tracing the cingulum bundle on T2-weighted MR images would be an alternative, but the resolution of those images was too poor too identify such a small white matter region. Placing an ROI box of constant size would reduce some of this bias, as well, but would introduce irrelevant pixels from gray matter or corpus callosum into our analysis. We attempted to mitigate this bias by tracing regions similar in shape to the cingulum bundle that we clearly identified and outlined on histological specimens. Though the lack of exact correspondence between the FA slices and histological slices (due to the far thicker 0.5 mm FA slices) made precise matching impossible, this likely resulted in less biased identification of the cingulum bundle on FA images. Even with our tracing method, however, the presence of pixels from gray matter or corpus callosum could affect mean measured FA, particularly in a small structure such as the cingulum bundle. Although this could not be avoided completely, careful ROI tracing reduces the number of incorrect pixels included. A more precise method for identifying the cingulum bundle on FA images would be to first trace white matter tracts using directional thresholding [15] and using those traces to pinpoint the cingulum bundle. This method, however, also introduces bias because it uses FA information to identify a region that will be used for FA comparisons.

In conclusion, our work failed to find a difference in either myelinated fiber length density or diffusion anisotropy in the cingulum bundle of MAG-knockout mice compared to wildtype controls. Our study was however limited by the low number of available mice, which may have influenced its outcome. We did, however, find corresponding decreases in both these measures with increasing age, which may be evidence for the physical alterations that underlie altered FA in DTI studies. Planned future studies include using electron microscopy to examine ultrastructural changes in oligodendrocytes and myelin sheaths at the single cell level in this model. Although it is likely that MAG dysfunction alone does not account for the ultrastructural and anisotropy alterations seen in schizophrenia but rather acts in conjunction with deficits in expression of other myelin-related genes [1], if ultrastructural studies were to show the same types of changes observed in brains from patients with schizophrenia, it may help validate the use of the MAG knockout mouse as a model for schizophrenia as well as shed new light on the processes that may be occurring in the disease.

Acknowledgements:

Supported by NIH grants MH66392 and MH82286. The study's sponsor played no role in study design, data analysis or interpretation, or paper preparation and submission.

The authors would like to thank Dr. C. Schmitz for helpful discussion, B. Wicinski and W.G.M. Janssen for expert technical assistance, and J. Ng and Y. Zhou for imaging assistance.

References

[1] Hakak Y., Walker J.R., Li C., Wong W.H., Davis K.L., Buxbaum J.D. et al., Genome-wide expression analysis reveals dysregulation of myelination-related genes in chronic schizophrenia, Proc Natl Acad Sci U S A, 2001; 98, 4746-4751

[2] Tkachev D., Mimmack M.L., Ryan M.M., Wayland M., Freeman T., Jones P.B. et al., Oligodendrocyte dysfunction in schizophrenia and bipolar disorder, Lancet, 2003; 362, 798-805

[3] Wan C., Yang Y., Feng G., Gu N., Liu H., Zhu S. et al., Polymorphisms of myelin-associated glycoprotein gene are associated with schizophrenia in the Chinese Han population, Neurosci Lett, 2005; 388, 126-131

[4] Hof P.R., Haroutunian V., Friedrich V.L., Jr., Byne W., Buitron C., Perl D.P. et al., Loss and altered spatial distribution of oligodendrocytes in the superior frontal gyrus in schizophrenia, Biol Psychiatry, 2003; 53, 1075-1085

[5] Uranova N.A., Vostrikov V.M., Orlovskaya D.D., Rachmanova V.I., Oligodendroglial density in the prefrontal cortex in schizophrenia and mood disorders: a study from the Stanley Neuropathology Consortium, Schizophr Res, 2004; 67, 269-275

[6] Uranova N., Orlovskaya D., Vikhreva O., Zimina I., Kolomeets N., Vostrikov V. et al., Electron microscopy of oligodendroglia in severe mental illness, Brain Res Bull, 2001; 55, 597-610

[7] Arnone D., McIntosh A.M., Tan G.M., Ebmeier K.P., Meta-analysis of magnetic resonance imaging studies of the corpus callosum in schizophrenia, Schizophr Res, 2008, 101, 124-132

[8] Highley J.R., Esiri M.M., McDonald B., Cortina-Borja M., Herron B.M., Crow T.J., The size and fibre composition of the corpus callosum with respect to gender and schizophrenia: a post-mortem study, Brain, 1999; 122 (Pt 1), 99-110

[9] Buchsbaum M.S., Friedman J., Buchsbaum B.R., Chu K.W., Hazlett E.A., Newmark R. et al., Diffusion tensor imaging in schizophrenia, Biol Psychiatry, 2006; 60, 1181-1187

[10] Buchsbaum M.S., Tang C.Y., Peled S., Gudbjartsson H., Lu D., Hazlett E.A. et al., MRI white matter diffusion anisotropy and PET metabolic rate in schizophrenia, NeuroReport, 1998; 9, 425-430

[11] Hoptman M.J., Ardekani B.A., Butler P.D., Nierenberg J., Javitt D.C., Lim K.O., DTI and impulsivity in schizophrenia: a first voxelwise correlational analysis, NeuroReport, 2004; 15, 2467-2470

[12] Kubicki M., McCarley R., Westin C.F., Park H.J., Maier S., Kikinis R. et al., A review of diffusion tensor imaging studies in schizophrenia, J Psychiatr Res, 2007; 41, 15-30

[13] Kubicki M., Park H., Westin C.F., Nestor P.G., Mulkern R.V., Maier S.E. et al., DTI and MTR abnormalities in schizophrenia: analysis of white matter integrity, Neuroimage, 2005; 26, 1109-1118

[14] Lim K.O., Hedehus M., Moseley M., de Crespigny A., Sullivan E.V., Pfefferbaum A., Compromised white matter tract integrity in schizophrenia inferred from diffusion tensor imaging, Arch Gen Psychiatry, 1999; 56, 367-374

[15] Miyata J., Hirao K., Namiki C., Fukuyama H., Okada T., Miki Y. et al., Interfrontal commissural abnormality in schizophrenia: tractography-assisted callosal parcellation, Schizophr Res, 2007; 97, 236-241

[16] Shergill S.S., Kanaan R.A., Chitnis X.A., O'Daly O., Jones D.K., Frangou S. et al., A diffusion tensor imaging study of fasciculi in schizophrenia, Am J Psychiatry, 2007; 164, 467-473

[17] Benes F.M., Emerging principles of altered neural circuitry in schizophrenia, Brain Res Rev, 2000; 31, 251-269

[18] Selemon L.D., Goldman-Rakic P.S., The reduced neuropil hypothesis: a circuit based model of schizophrenia, Biol Psychiatry, 1999; 45, 17-25

[19] Devinsky O., Morrell M.J., Vogt B.A., Contributions of anterior cingulate cortex to behaviour, Brain, 1995; 118 (Pt 1), 279-306

[20] Dracheva S., Davis K.L., Chin B., Woo D.A., Schmeidler J., Haroutunian V., Myelin-associated mRNA and protein expression deficits in the anterior cingulate cortex and hippocampus in elderly schizophrenia patients, Neurobiol Dis, 2006; 21, 531-540

[21] Katsel P., Davis K.L., Haroutunian V., Variations in myelin and oligodendrocyte-related gene expression across multiple brain regions in schizophrenia: a gene ontology study, Schizophr Res, 2005; 79, 157-173

[22] McCullumsmith R.E., Gupta D., Beneyto M., Kreger E., Haroutunian V., Davis K.L. et al., Expression of transcripts for myelination-related genes in the anterior cingulate cortex in schizophrenia, Schizophr Res, 2007; 90, 15-27

[23] Stark A.K., Uylings H.B., Sanz-Arigita E., Pakkenberg B., Glial cell loss in the anterior cingulate cortex, a subregion of the prefrontal cortex, in subjects with schizophrenia, Am J Psychiatry, 2004; 161, 882-888

[24] Yakovlev P.I., Locke S., Limbic nuclei of thalamus and connections of limbic cortex. III. Corticocortical connections of the anterior cingulate gyrus, the cingulum, and the subcallosal bundle in monkey, Arch Neurol, 1961; 5, 364-400

[25] Schmahmann J.D., Pandya D.N., Wang R., Dai G., D'Arceuil H.E., de Crespigny A.J. et al., Association fibre pathways of the brain: parallel observations from diffusion spectrum imaging and autoradiography, Brain, 2007; 130, 630-653

[26] Kubicki M., Westin C.F., Nestor P.G., Wible C.G., Frumin M., Maier S.E. et al., Cingulate fasciculus integrity disruption in schizophrenia: a magnetic resonance diffusion tensor imaging study, Biol Psychiatry, 2003; 54, 1171-1180

[27] Sun Z., Wang F., Cui L., Breeze J., Du X., Wang X. et al., Abnormal anterior cingulum in patients with schizophrenia: a diffusion tensor imaging study, NeuroReport, 2003; 14, 1833-1836

[28] Wang F., Sun Z., Cui L., Du X., Wang X., Zhang H. et al., Anterior cingulum abnormalities in male patients with schizophrenia determined through diffusion tensor imaging, Am J Psychiatry, 2004; 161, 573-575

[29] Fujiwara H., Namiki C., Hirao K., Miyata J., Shimizu M., Fukuyama H. et al., Anterior and posterior cingulum abnormalities and their association with psychopathology in schizophrenia: a diffusion tensor imaging study, Schizophr Res, 2007; 95, 215-222

[30] Segal D., Haznedar M.M., Hazlett E.A., Entis J.J., Newmark R.E., Torosjan Y. et al., Diffusion tensor anisotropy in the cingulate gyrus in schizophrenia, Neuroimage, 2010; 50, 357-365

[31] Kumra S., Ashtari M., Cervellione K.L., Henderson I., Kester H., Roofeh D. et al., White matter abnormalities in early-onset schizophrenia: a voxel-based diffusion tensor imaging study, J Am Acad Child Adolesc Psychiatry, 2005; 44, 934-941

[32] White T., Cullen K., Rohrer L.M., Karatekin C., Luciana M., Schmidt M. et al., Limbic structures and networks in children and adolescents with schizophrenia, Schizophr Bull, 2008; 34, 18-29

[33] Li C., Tropak M.B., Gerlai R., Clapoff S., Abramow-Newerly W., Trapp B. et al., Myelination in the absence of myelin-associated glycoprotein, Nature, 1994; 369, 747-750

[34] Loers G., Aboul-Enein F., Bartsch U., Lassmann H., Schachner M., Comparison of myelin, axon, lipid, and immunopathology in the central nervous system of differentially myelin-compromised mutant

mice: a morphological and biochemical study, Mol Cell Neurosci, 2004; 27, 175-189

[35] Weiss M.D., Hammer J., Quarles R.H., Oligodendrocytes in aging mice lacking myelin-associated glycoprotein are dystrophic but not apoptotic, J Neurosci Res, 2000; 62, 772-780

[36] Weiss M.D., Luciano C.A., Quarles R.H., Nerve conduction abnormalities in aging mice deficient for myelin-associated glycoprotein, Muscle Nerve, 2001; 24, 1380-1387

[37] Montag D., Giese K.P., Bartsch U., Martini R., Lang Y., Bluthmann H. et al., Mice deficient for the myelin-associated glycoprotein show subtle abnormalities in myelin, Neuron, 1994; 13, 229-246

[38] Pan B., Fromholt S.E., Hess E.J., Crawford T.O., Griffin J.W., Sheikh K.A. et al., Myelin-associated glycoprotein and complementary axonal ligands, gangliosides, mediate axon stability in the CNS and PNS: neuropathology and behavioral deficits in single- and double-null mice, Exp Neurol, 2005; 195, 208-217

[39] Quarles R.H., A hypothesis about the relationship of myelin-associated glycoprotein's function in myelinated axons to its capacity to inhibit neurite outgrowth, Neurochem Res, 2009; 34, 79-86

[40] Hoistad M., Segal D., Takahashi N., Sakurai T., Buxbaum J.D., Hof P.R., Linking white and grey matter in schizophrenia: oligodendrocyte and neuron pathology in the prefrontal cortex, Front Neuroanat, 2009; 3, 9

[41] Zhang J., van Zijl P.C., Mori S., Three-dimensional diffusion tensor magnetic resonance microimaging of adult mouse brain and hippocampus, Neuroimage, 2002; 15, 892-901

[42] Hof P.R., Young W.G., Bloom F.E., Belichenko P.V., Celio M.R. Comparative Cytoarchitectonic Atlas of the C57BL/6 and 129/Sv Mouse Brains. Amsterdam: Elsevier; 2000.

[43] Schmued L., Slikker W., Jr., Black-gold: a simple, high-resolution histochemical label for normal and pathological myelin in brain tissue sections, Brain Res, 1999; 837, 289-297

[44] Calhoun M.E., Mouton P.R., Length measurement: new developments in neurostereology and 3D imagery, J Chem Neuroanat, 2001; 21, 257-265

[45] Kreczmanski P., Schmidt-Kastner R., Heinsen H., Steinbusch H.W., Hof P.R., Schmitz C., Stereological studies of capillary length density in the frontal cortex of schizophrenics, Acta Neuropathol, 2005; 109, 510-518

[46] Mouton P.R., Gokhale A.M., Ward N.L., West M.J., Stereological length estimation using spherical probes, J Microsc, 2002; 206, 54-64

[47] Schmitz C., Hof P.R., Design-based stereology in neuroscience, Neuroscience, 2005; 130, 813-831

[48] Schmitz C., Grolms N., Hof P.R., Boehringer R., Glaser J., Korr H., Altered spatial arrangement of layer V pyramidal cells in the mouse brain following prenatal low-dose X-irradiation. A stereological study using a novel three-dimensional analysis method to estimate the nearest neighbor distance distributions of cells in thick sections, Cereb Cortex, 2002; 12, 954-960

[49] Davis K.L., Stewart D.G., Friedman J.I., Buchsbaum M., Harvey P.D., Hof P.R. et al., White matter changes in schizophrenia: evidence for myelin-related dysfunction, Arch Gen Psychiatry, 2003; 60, 443-456

[50] Kubicki M., McCarley R.W., Shenton M.E., Evidence for white matter abnormalities in schizophrenia, Curr Opin Psychiatry, 2005; 18, 121-134

[51] Highley J.R., Esiri M.M., McDonald B., Roberts H.C., Walker M.A., Crow T.J., The size and fiber composition of the anterior commissure with respect to gender and schizophrenia, Biol Psychiatry, 1999; 45, 1120-1127

[52] Chance S.A., Highley J.R., Esiri M.M., Crow T.J., Fiber content of the fornix in schizophrenia: lack of evidence for a primary limbic encephalopathy, Am J Psychiatry, 1999; 156, 1720-1724

[53] Marner L., Pakkenberg B., Total length of nerve fibers in prefrontal and global white matter of chronic schizophrenics, J Psychiatr Res, 2003; 37, 539-547

[54] Highley J.R., Walker M.A., Esiri M.M., Crow T.J., Harrison P.J., Asymmetry of the uncinate fasciculus: a post-mortem study of normal subjects and patients with schizophrenia, Cereb Cortex, 2002; 12, 1218-1224

[55] Casanova M.F., Zito M., Bigelow L.B., Berthot B., Sanders R.D., Kleinman J.E., Axonal counts of the corpus callosum of schizophrenic patients, J Neuropsychiatry Clin Neurosci, 1989; 1, 391-393

[56] Nasrallah H.A., McCalley-Whitters M., Bigelow L.B., Rauscher F.P., A histological study of the corpus callosum in chronic schizophrenia, Psychiatry Res, 1983; 8, 251-260

[57] Segal D., Schmitz C., Hof P.R., Spatial distribution and density of oligodendrocytes in the cingulum bundle are unaltered in schizophrenia, Acta Neuropathol, 2009; 117, 385-394

[58] Peters A., The effects of normal aging on myelin and nerve fibers: a review, J Neurocytol, 2002; 31, 581-593

[59] Voineskos A.N., Lobaugh N.J., Bouix S., Rajji T.K., Miranda D., Kennedy J.L. et al., Diffusion tensor tractography findings in schizophrenia across the adult lifespan, Brain, 2010; 133, 1494-1504

[60] Kaufman J.A., Ahrens E.T., Laidlaw D.H., Zhang S., Allman J.M., Anatomical analysis of an aye-aye brain (D*aubentonia madagascariensis, Primates: Prosimii*) combining histology, structural magnetic resonance imaging, and diffusion-tensor imaging, Anat Rec, 2005; 287A, 1026-1037